Agricultural and Forest Meteorology 150 (2010) 182–195

Contents lists available at ScienceDirect

Agricultural and Forest Meteorology

journal homepage: www.elsevier.com/locate/agrformet

A comparative study of a multilayer and a productivity (light-use) efficiency land-surface model over different temporal scales

Paul Alton *, Per Bodin

Geography Dept., University of Swansea, Swansea, Wales SA2 8PP, UK

ARTICLE INFO

Article history:
Received 16 February 2009
Received in revised form 5 October 2009
Accepted 9 October 2009

Keywords:
Radiative transfer
Light-use efficiency
Eddy-covariance
Global carbon cycle
Model comparison
Model inversion

ABSTRACT

Several recent studies suggest that a simple productivity efficiency model (PEM), based on daily or weekly light-use efficiency, is sufficient to represent the exchange of carbon, water and energy at the land-surface. At the same time, many global land-surface models are becoming more process-based, simulating at high temporal resolution the interception of direct and diffuse sunlight at different depths within the canopy. Quantifying the accuracy and limitations of both types of model has become of great importance. The current study compares a PEM with a more complex (and computationally expensive) multilayer model operating at timesteps as short as 30 min (JULES-SF). Each model is optimised against observed fluxes (net carbon exchange, latent heat, sensible heat and net radiation) within the FLUXNET archive for an unprecedented number of sites (30) and site-years (71). Our main finding is that, after optimisation, the process-based multilayer model performs significantly better than the PEM on all timescales (daily and seasonal). However, the difference in model performance appears to diminish with an increase in measurement timescale. Thus, on average, the modelling efficiency increases from 0.32 (daily) to 0.46 (seasonal) using the PEM approach ($r^2 = 0.53 \rightarrow 0.71$), whilst it remains close to 0.6 for JULES-SF on both timescales ($r^2 = 0.69 \rightarrow 0.75$). We find that the maximum number of biophysical parameters that can be tuned against site fluxes (4 observables) is quite limited (typically 3–4). This inference applies to both models despite their considerable difference in complexity.

© 2009 Elsevier B.V. All rights reserved.

1. Introduction

Global land-surface models (LSMs) traditionally adopt simple algorithms for reasons of computational expediency (Raupach and Finnigan, 1988; Sellers et al., 1996a, 1997). Recently, however, some global LSMs have increased in complexity, especially with respect to canopy light-interception (Dai et al., 2004; Alton et al., 2007b; Mercado et al., 2009). This change is in recognition of the important role played by cloud and diffuse sunlight in the accurate predictions of carbon, water and energy exchange (Gu et al., 1999; Roderick et al., 2001; Gu et al., 2002; Lyons, 2002; Niyogi et al., 2004). At the same time, some authors find simple empirical LSMs, once calibrated against observations, provide sufficient accuracy for most purposes. For example, the productivity efficiency model (light-use efficiency or epsilon model), which is forced by daily, weekly or monthly climate, and takes no explicit account of vertical canopy structure, is shown to reproduce Gross Primary Productivity (GPP) fairly well at several carbon-monitoring eddy-covariance sites at least on longer (weekly and monthly) timescales (Medlyn et al., 2003; Sims et al., 2005; Yuan et al., 2007). Such models are well suited to available satellite data. Indeed, a PEM algorithm allows global GPP to be derived on a daily basis using MODIS estimates of absorbed photosynthetically active radiation (PAR; Running et al., 2004; Zhao et al., 2005; Heinsch et al., 2006. A coarse timestep is also better suited to currently available meteorological forcing data although reconstructed datasets on shorter (3-hourly) timesteps are starting to become available (Dirmeyer et al., 1999; Sheffield et al., 2006).

All global LSMs, especially the more process-based, require a large number of input biophysical parameters to represent carbon, water and energy exchange at the vegetated land-surface. For example, the Met.Office Surface Exchange Scheme (MOSES; Cox et al., 1999) and the Lund-Potsdam-Jena model (LPJ; Zaehle et al., 2005) contain, about 50 and 40 parameters, respectively. Within the model, many of these parameters assume different values according to biome or Plant Functional Type (PFT). Although field measurements are available for parameterization of global LSMs, many biophysical properties are not well known across all PFTs (Sellers et al., 1995). A considerable advantage of the PEM-approach is that it reduces significantly the number of prescribed parameters.

One way to use a LSM is to optimise against site fluxes and then scale globally. Indeed, Falge et al. (2002) emphasize the urgent

* Corresponding author.
E-mail address: p.alton@swansea.ac.uk (P. Alton).

0168-1923/$ – see front matter © 2009 Elsevier B.V. All rights reserved.
doi:10.1016/j.agrformet.2009.10.001

need to calibrate global LSMs more rigorously in this way. The recent expansion of the FLUXNET archives (Baldocchi et al., 2001; Falge et al., 2002) provides a long-awaited opportunity to calibrate global LSMs against carbon, water and energy fluxes recorded at a large number of sites and for several PFTs.

In this study, we calibrate two global land-surface models by comparing model output against observed carbon, water and energy fluxes from 30 sites (71 site-years) contained in the Marconi FLUXNET archive. The two models span a large range in complexity. The simpler model is forced with daily climate and yields GPP according to light-use efficiency. The more complex model is a process-based approach forced by half-hourly climate which takes account of changes in leaf nitrogen, microclimate and light interception with depth through the canopy. It has recently been enhanced to take explicit account of leaf orientation, diffuse sky radiance and sunfleck penetration, and is therefore one of the most complex LSMs that operate globally, at least in terms of canopy light-interception (Alton et al., 2005, 2007a,b). For both models, the most influential parameters are determined by sensitivity analysis and then optimised to produce closest agreement with observed carbon, water and energy fluxes recorded at site-level. The main scientific research question can be summarised as follows: once optimised, how accurately can each of the LSMs reproduce site-level carbon, water and energy fluxes measured over different timescales (half-hourly, daily and seasonally) and by how much does the process-based, multilayer model perform better than the simple PEM?

2. Methods and materials

The methodology consists of two main parts: (1) a sensitivity analysis to determine the most influential parameters within the model; and (2) the use of FLUXNET archival data to optimise (tune) the model and to assess its performance at site-level. The two parts are carried out for a relatively simple productivity efficiency model (JULES-PEM) and a more complex, multilayer, process-based model (JULES-SF). The following sections describe the models (Section 2.1), the datasets (Section 2.2) and the two parts of the methodology (Section 2.3).

2.1. Land-surface modelling

The more complex model (JULES-SF) is based on the Met.Office Surface Exchange Scheme (MOSES; Cox et al., 1999), after a series of enhancements (Alton et al., 2007a; Mercado et al., 2007; Alton, 2008). Detail for the land-surface model, including important equations, are contained in Appendix A. Here we focus on the main differences between JULES-SF and JULES-PEM which concern primarily the representation of the canopy.

The energy calculation central to JULES (Joint UK Land Environmental Simulator) is the Penman–Monteith approach (Monteith, 1965), ensuring the balance of ingoing and outgoing fluxes at the land-surface. Within JULES-SF, stomatal conductance, transpiration and photosynthesis are calculated in each of five leaf layers, before summing to produce total values for the entire canopy (Alton et al., 2007a; Mercado et al., 2007). Enhancements for sunfleck penetration, explicit leaf orientation and diffuse sunlight permit a more realistic canopy response under both direct sunlight and cloud (Alton et al., 2005, 2007a). Leaf photosynthesis for the C_3 and C_4 pathways are derived using the co-limitation model of Collatz et al. (1991, 1992) which is conceptually similar to the biochemical model of Farquhar et al. (1980). Input to the model consists of meteorological (forcing) driving data, LAI phenology and biophysical parameters. We use the AVHRR (satellite-derived) LAI which possesses a 10-day temporal resolution and a spatial resolution of 0.25° or ~20 km (Los et al., 2000). The satellite timeseries is normalised so that the peak, growing season LAI is equal to $LAI_{\max}$. $LAI_{\max}$ is a PFT-specific parameter and is included in the parameter sensitivity analysis discussed below.

To create the productivity efficiency model (JULES-PEM) we use the same soil hydrology and soil respiration as JULES-SF. However, we make the following simplifications with respect to canopy, surface reflectance and climatic forcing:

1. Canopy GPP is estimated according to total solar irradiance and light-use efficiency (LUE; Monteith, 1977; Gower et al., 1999; Medlyn et al., 2003; Yuan et al., 2007):

$$GPP = \epsilon \times fPAR \times I_{PAR} \times FSMC \times FT \quad (1)$$

where ϵ is the potential light-use efficiency (g m^{-2} MW^{-1}), I_{PAR} is the PAR incident at the top of the canopy (MW^{-1}) and fPAR is the fraction of absorbed PAR. Eq. (1) replaces an estimation of gross productivity within each leaf layer before summing all layers to produce GPP for the entire canopy. The stresses on leaf productivity owing to temperature and soil moisture content, FT and FSMC in Eq. (1), remain as before (Appendix A).

2. To simplify the calculation of autotrophic respiration, the carbon use efficiency (CUE) is prescribed:

$$CUE = \frac{NPP}{GPP} \quad (2)$$

where NPP is the net primary productivity (Running and Coughlan, 1988; Waring et al., 1998; de Lucia et al., 2007). This replaces the calculation of leaf respiration within each canopy layer, based on foliar temperature and nitrogen content, which is then scaled in JULES-SF according to the ratios of plant-to-leaf nitrogen and growth-to-maintenance respiration to yield total autotrophic respiration (Eqs. (11) and (13) in Appendix A). Within the literature, PEMs are adopted for both GPP (Choudhury, 2001; Medlyn et al., 2003; Heinsch et al., 2006; Yuan et al., 2007) and NPP (Potter et al., 1993; Goetz and Prince, 1996; Gower et al., 1999; Ruimy et al., 1999; Barrett, 2002; Running et al., 2004). The implementation within JULES-PEM of both CUE and ϵ permits comparison with both types of model.

3. The vertical gradients in leaf nitrogen, photosynthetic capacity and boundary-layer resistance are not modelled within JULES-PEM. Total stomatal conductance of the canopy (g_c; mol m^{-2} s^{-1}) is estimated via the diffusion equation:

$$g_c = \frac{A_c}{c_a - c_i} \quad (3)$$

where A_c and c_a are, respectively, the canopy net productivity (mol m^{-2} s^{-1}) and the ambient CO_2 concentration (mol mol^{-1}; e.g. Cox et al., 1998). The quantity c_i (mol mol^{-1}) is the leaf CO_2 concentration which is often observed to be constant over a wide range of conditions (Wong et al., 1979; Long and Hutchin, 1991; Campbell and Norman, 1998, although see Houborg et al., in press). It is now prescribed as an input parameter, rather than calculated as an internal variable using the Ball–Berry relation (Eq. (14) in Appendix A). A_c follows from GPP- R_L where the total leaf respiration within the canopy, R_L, is given by:

$$R_L = \frac{R_{PM}}{PL} = \frac{GPP}{PL} \times \frac{1 - CUE - R_{grow}}{1 - R_{grow}} \quad (4)$$

where R_{PM}, PL and R_{grow} are, respectively, the plant maintenance respiration, the plant-to-leaf nitrogen ratio and the growth-to-maintenance ratio (Appendix A). Note that we constrain $R_L \geq 0$ in Eq. (4) (otherwise R_L is negative when CUE is very high) and g_c=0 when $R_L \geq GPP$ (stomatal closure).

4. No account is taken of the directionality of solar radiance (diffuse/direct). Albedo pertaining to the whole surface (soil + vegetation) is prescribed for the visible and near-infrared wavebands via the parameters *albpar* and *albnir*, respectively. This replaces the two-stream calculation based on soil albedo, LAI and leaf optical properties (Sellers et al., 1996a).
5. A daily climatology is employed by averaging the half-hourly climatology used in the complex model.

In summary, 5 parameters introduced into JULES-PEM replace 15 parameters required for JULES-SF. Parameters are assigned default values from the literature in Table 1 whilst the salient differences between JULES-SF and JULES-PEM are summarised in Table 2. Whilst it might have been possible to employ a pre-existing PEM to compare with JULES-SF, our chosen method ensures that any differences between the models, in terms of performance and behaviour, can be attributed to the simplifications we have made rather than the diverse origin and construction of each model. Such a modular approach is advocated by Knorr and Heimann (2001). We recognise that our chosen PEM is simple and that, within at least one recent version of the PEM, a more elaborate calculation of canopy stomatal conductance

Table 1
Default (literature) values for the input biophysical parameters. Where there are sufficient data to indicate significant differences amongst PFTs, values are given in the following order: broadleaf forest (BL), needleleaf forest (NL), C_3 grassland (C_3), C_4 grassland (C_4) and tundra shrubland (SH). Default values and their uncertainties are taken from the following sources and references therein: Baldocchi and Harley (1995) for parameters 1 and 2; main text for 3 (Section 2.2); Cox (2001) and Alton et al. (2007a) for 4; Law et al. (2002) and Asner et al. (2003) for 5; Cosby et al. (1984) and Dirmeyer et al. (1999) for 6–11; Barnsley (2007) for 12; Newman (1969) for 13; Ramirez and Senarath (2000) for 14; Jackson et al. (1996) for 16; Collatz et al. (1991) and Sellers et al. (1996a,b) for 17 and 18; Tjoelker et al. (2001) for 19; Schlesinger (1997) for 20; Raich and Schlesinger (1992) for 21; Singsaas et al. (2001) for 22; Williams (1991) for 23 and 24; Farquhar et al. (1980); Lloyd et al. (2002); Law et al. (1999); Bolstad et al. (2004) for 25; Field and Mooney (1986); Schulze et al. (1994); Meir et al. (2002) for 26 and 27; Bolstad et al. (2004); Law et al. (1999); Lloyd et al. (2002); Ryan (1991a) for 28; Williams (1991) for 29 and 30; Ryan (1991b) for 31; Campbell and ?Schrader et al. (2004); Hendrickson et al. (2004); Al-Khatib and Paulsen (1999) for 32 and 33; Carswell et al. (2000); Lewis et al. (2000); Meir et al. (2002); Dang et al. (1998) for 34; Udo and Aro (1999) for 35; Misson et al. (2004); Sellers et al. (1996a,b) for 36 and 37, Campbell and Norman (1998) for 38, Yuan et al. (2007) for 39, Wong et al. (1979) for 40, de Lucia et al. for 41, Barnsley (2007) for 42 and 43. PAR, NIR and LAI are, respectively, photosynthetically active radiation, near-infrared radiation and Leaf Area Index.

Number	Model(s)	Name	Value	Uncertainty	Units	Description
1	SF/PEM	$z1_u$	10	5	m	Height above canopy for measurement of wind speed
2	SF/PEM	$z1_t$	10	5	m	Height above canopy for measurement of temperature & humidity
3	SF/PEM	SMC_i	0.62	0.11	–	Initial soil moisture as fraction of saturation
4	SF/PEM	h	25 20 1 1 2	5 5 0.5 0.5 1.0	m	Height to top of canopy
5	SF/PEM	LAI_{max}	4.3 4.4 3.1 3.1 1.5	1.4 2.3 1.4 1.4 0.5	m	Peak LAI of growing season
6	SF/PEM	b	7	4	–	Clapp–Hornberger exponent
7	SF/PEM	sathh	0.035	0.015	m	Absolute soil matric suction at saturation
8	SF/PEM	satcon	0.0073	0.0037	$mm\,s^{-1}$	Hydraulic conductivity at saturation
9	SF/PEM	SMCV	0.42	0.04	$m^3\,m^{-3}$	Volumetric soil moisture at saturation
10	SF/PEM	hcap	1.26e6	0.07e6	$Jm^{-3}\,K^{-1}$	Dry heat capacity of soil
11	SF/PEM	hcon	0.27	0.05	$Wm^{-1}\,K^{-1}$	Dry thermal conductivity of soil
12	SF	a_g	0.18	0.08	–	Soil albedo for solar radiation
13	SF/PEM	ψ_c	−200	100	m	Critical potential for soil moisture stress
14	SF/PEM	dcatch0	0.2	0.1	$kg\,m^{-2}$	Change in water-holding capacity w.r.t. LAI
15	SF	infil	4 4 2 2 2	1	–	Enhancement factor for infiltration of top soil
16	SF/PEM	D_r	0.33 0.33 0.2 0.2 0.11	0.05	m	Root exponential scale-depth
17	SF	β_1	0.89	0.09	–	Light-Rubisco photosynthetic co-limitation factor
18	SF	β_2	0.89	0.09	–	Sucrose photosynthetic co-limitation factor
19	SF/PEM	Q_{10}(leaf)	2.3	0.5	–	Fractional change in leaf respiration per 10 K change in temperature
20	SF/PEM	κ	1.8e −8	1.3e −8	$kg\,m^{-2}\,s^{-1}$	Decompositional rate of soil carbon
21	SF/PEM	Q_{10}(soil)	2.3	0.7	–	Fractional change in soil decomposition per 10 K change in temperature
22	SF	QE	0.07	0.02	$mol\,mol^{-1}$	Top-of-canopy quantum efficiency to absorbed PAR
23	SF	R_{NIR}	0.50	0.05	–	Leaf reflectance in NIR waveband
24	SF	R_{PAR}	0.10	0.05	–	Leaf reflectance in PAR waveband
25	SF	F_d	0.020	0.015	–	Leaf dark respiration as fraction of leaf photosynthetic capacity (V_{cmax})
26	SF	N_{eff}	28	16	$\mu\,mol\,g^{-1}\,s^{-1}$	Ratio V_{cmax} ($\mu\,mol\,m^{-2}\,s^{-1}$) to leaf nitrogen ($g\,m^{-2}$)
27	SF	N_a	3.0 3.0 1.5 1.5 3.0	1.0 1.0 0.5 0.5 1.0	$g\,m^{-2}$	Leaf nitrogen content
28	SF/PEM	PL	8 4 4 4 4	3 1.6 1.6 1.6 1.6	–	Ratio of plant-to-leaf nitrogen
29	SF	T_{PAR}	0.05	0.05	–	Leaf transmittance in the PAR waveband
30	SF	T_{NIR}	0.30	0.15	–	Leaf transmittance in the NIR waveband
31	SF/PEM	R_{grow}	0.25	0.10	–	Ratio growth to maintenance respiration
32	SF/PEM	T_l	5	10	°C	Lower inhibition temperature for photosynthesis
33	SF/PEM	T_h	40	10	°C	Upper inhibition temperature for photosynthesis
34	SF	k_{rub}	0.15	0.10	–	Nitrogen allocation exponential coefficient
35	SF/PEM	PS	0.50	0.05	–	Fraction of sky irradiance which is PAR
36	SF	g_{min}	0.03	0.02	$mol\,m^{-2}\,s^{-1}$	Intercept of the Ball-Berry stomatal model
37	SF	m	8	4	–	Slope of the Ball–Berry stomatal model
38	SF/PEM	dz_m	0.05 0.05 0.1 0.1 0.1	0.025 0.025 0.05 0.05 0.05	$m\,m^{-1}$	Change in roughness length with canopy height
39	PEM	ϵ	2	1	$g\,m^{-2}\,MW^{-1}$	Potential light-use efficiency
40	PEM	c_i	20	8	Pa	Leaf internal CO_2 concentration
41	PEM	CUE	0.5	0.3	–	Carbon-use efficiency (net to primary productivity ratio)
42	PEM	albpar	0.20	0.15	–	Surface albedo in PAR waveband
43	PEM	albnir	0.40	0.30	–	Surface albedo in NIR waveband

Table 2
Primary differences between the two land-surface models. PAR, NIR and CUE denote, respectively, photosynthetically active radiation, near-infrared radiation and carbon-use efficiency.

Model attribute	JULES-SF	JULES-PEM
Canopy representation	Multilayer	Single layer
GPP	Biochemical co-limitation (Eqs. (8)–(11))	Light-use efficiency (Eq. (1))
Stomatal conductance	Ball–Berry relation (Eq. (14))	Diffusion equation (Eq. (3))
Surface albedo	Two-stream calculation Sellers et al., 1996a	Prescribed for PAR and NIR
Plant respiration	Maintenance and growth terms (Eqs. (12) and (13))	Prescribed via CUE (Eq. (2))
Meteorological forcing	Half-hourly	Daily average

is implemented (Anderson et al., 2000; Houborg et al., in press). In general, however, the PEM is used for estimation of carbon assimilation and our corresponding equations (Eqs. (1) and (2)) are applied widely within this context.

2.2. Observational data

Carbon, water and energy exchange are simulated at FLUXNET sites in order to determine the sensitivity to input parameters and to optimise the most influential parameters within the model. Half-hourly measurements of site meteorology, carbon Net Ecosystem Exchange (NEE), latent heat (LE), sensible heat (H) and net radiation (Rn) are extracted from the Marconi FLUXNET archive (Baldocchi et al., 2001). Gap-filled data (Falge et al., 2002) are used for meteorological variables, since the LSM requires a continuous forcing, but not for observed fluxes. Observed fluxes originate from 38 sites and cover 98 site-years. The Marconi archive is biased towards forests of Europe and N. America but it covers a diverse range of PFTs. Each site-year is ascribed to one of 5 PFTs defined within the model, namely: broadleaf trees (BL), needleleaf trees (NL), C_3 grassland (C_3), C_4 grassland (C_4) and shrubs (SH). For the 6 site-years of mixed forest (MX) we assume 50% broadleaf and 50% needleleaf. A summary of location and vegetational composition is given in Table 3.

The analysis is limited to the growing season (typically Day of the Year 135–255) since, outside this period, the site meteorology is often incomplete. In all, 30 sites from Table 3 fit this condition, yielding a total of 71 site-years. Tests with site-years possessing an unbroken meteorology throughout the year, suggest that our results do not change significantly if we adopt an analysis period more extended than the growing season. Soil moisture measurements are sparse within the Marconi archive. Therefore, in order to initialise soil moisture within the model, we use the spin-up from global simulations conducted previously with JULES-SF (Alton et al., in press) and extract the initial soil moisture content for the Marconi locations at the beginning of the growing season. This initial soil moisture content, used to initialise all four soil layers within the model, is included as a tuneable parameter (SMC_i) within the sensitivity analysis.

2.3. Methodology

(1) Sensitivity analysis

In order to determine model sensitivity and optimise the LSM we calculate chi squared (χ^2). Thus, for each PFT, we compute:

$$\chi^2 = \sum_{i=1}^{n} \frac{(F_{sim} - F_{obs})^2}{(\Delta F_{obs})^2} \quad (5)$$

Table 3
Summary of sites and site-years available in the Marconi FLUXNET archive Falge et al., 2002. Plant Functional Types (PFTs) defined in the model are broadleaf forest (BL), needleleaf forest (NL), C_3 grassland (C_3), C_4 grassland (C_4) and tundra shrubland (SH). MX denotes mixed broadleaf/needleleaf forest. Sites used for model optimisation are denoted by an asterisk. Law et al. (2002) provide a more complete description of the Marconi sites with references to the original publication of data.

Site	Latitude (°N)	Longitude (°E)	PFT	Year(s)
Manaus, Brazil	−1.4	−59.8	BL*	1996,1999
Gunnarsholt, Iceland	63.8	−20.2	BL*	1996–1998
Hesse, France	48.7	7.1	BL*	1996–1999
Harvard, USA	42.0	−72.2	BL*	1992–1999
Soroe, Denmark	55.4	11.7	BL*	1996–1999
Vielsalm, Belgium	50.3	6.0	BL*	1997–1998
Walker Branch, USA	35.9	−84.3	BL*	1995–1998
Willow Creek, USA	45.8	−90.1	BL*	1997–1999
Castelporziano, Italy	41.8	12.4	BL*	1997–1998
Sky Oaks (old), USA	33.4	−116.6	BL	1997–2000
Sky Oaks (young), USA	33.4	−116.6	BL	1997–2000
Aberfeldy, Scotland	56.6	−3.8	NL*	1997–1998
Blodgett Forest, USA	38.9	−120.6	NL*	1997–1999
Duke, USA	36.0	−79.1	NL	1998–1999
Flakaliden, Sweden	64.1	19.5	NL*	1996–1998
Howland, USA	45.2	−68.7	NL	1996–1997
Hyytiala, Finland	61.9	24.3	NL*	1996–1998
Saskatchewan, Canada	53.9	−104.7	NL	1994
Loobos, Netherlands	52.2	5.8	NL*	1996–1998
Metolius, USA	44.5	−121.6	NL*	1996–1997
Manitoba, Canada	55.9	−98.5	NL*	1994–1998
Norunda, Sweden	60.1	17.5	NL*	1996–1998
Niwot Ridge, USA	40.0	−105.6	NL*	1999
Tharandt, Germany	51.0	13.6	NL*	1996–1999
Weidenbrunnen, Germany	50.2	11.8	NL*	1996
Wind River, USA	45.8	−121.9	NL*	1998
Zotino, Siberia	60.8	89.4	NL*	1999
Braschaat, Belgium	51.3	4.5	MX*	1996–1998
Park Falls, USA	45.9	−90.2	MX*	1999
Ponca City, USA	36.8	−97.0	C_3*	1997
Bondville, USA	40.0	−88.3	C_3/C_4*	1997–1999
Little Washita, USA	35.0	−97.9	C_4*	1997–1997
Shidler, USA	36.9	−96.6	C_4*	1997
Barrow, USA	70.3	−156.6	SH*	1998–1999
Happy Valley, USA	69.1	−148.8	SH*	1994–1995
Upad, USA	70.3	−148.8	SH	1994

where summation takes place over all fluxes (NEE, LE, H and Rn) from all site-years relevant to the PFT. The simulated (F_{sim}) and observed (F_{obs}) fluxes are half-hourly for JULES-SF and daily (24 h) for JULES-PEM. The error in the observed flux (ΔF_{obs}) is poorly defined and, for half-hourly fluxes we estimate it as follows. Observed fluxes are grouped into 10-day composites, the approximate timescale over which fluxes are observed to change due to physiology and the influence of soil moisture (Goulden et al., 1996). We also use downwelling shortwave radiation, one of the main drivers of atmosphere-landsurface exchange (Hollinger et al., 1994; Knohl and Baldocchi, 2008) to aggregate the data by adopting a bin width of 50 W m^{-2}. The standard deviation about the mean of each bin is used as a measure of observational error. Although this approach is likely to overestimate the true error, as any variation in the flux unrelated to shortwave radiation is attributed to measurement uncertainty, the values thus derived (Table 4) are close to previous estimates (Goulden et al., 1996; Medlyn et al., 2005). It is difficult to estimate daily ΔF_{obs} for JULES-PEM since daily values of shortwave radiation vary considerably over the 10-day composite. Consequently, we adopt ΔF_{obs} from the half-hourly measurements scaled to the same units as daily F_{obs}. This overestimates the error in the daily fluxes but we argue that this is acceptable since we are not comparing models in this part of the methodology. Indeed, the model comparisons we conduct later rely on the variance in the observations and do not depend on our estimates of ΔF_{obs} at all. The identification of the most influential

Table 4
Errors assumed for the observed half-hourly fluxes of Net Ecosystem Exchange (NEE), latent heat (LE), sensible heat (H) and net radiative exchange (Rn). Plant Functional Types (PFTs) are designated as in Table 3.

PFT	NEE (μmol m^{-2} s^{-1})	LE (W m^{-2})	H (W m^{-2})	Rn (W m^{-2})
BL	3.2	36	32	39
NL	3.0	27	35	37
C_3	2.7	35	26	26
C_4	3.4	37	25	22
SH	1.2	16	20	20
MX	2.7	39	33	23

parameters, as well as their optimisation, rely only on the *relative* change in χ^2 between simulations and are therefore fairly insensitive to ΔF_{obs}. This is confirmed by replacing ΔF_{obs} by the mean observed flux in Eq. (5), as suggested by Reichstein et al. (2003). This substitution does not change our ranking of the most influential parameters nor the final parameter values determined from the optimisation. To ensure that observed flux is not grossly underestimated, we exclude measurements from Eq. (5) where the frictional velocity is too low ($<$0.16 m s^{-1}; Goulden et al., 1996; Reichstein et al., 2003). Where frictional velocity is not recorded, we exclude fluxes where windspeed $<$2 m s^{-1} (Medlyn et al., 2003). Fluxes excluded on the basis of either low turbulent flow or gap-filling (i.e. missing in the original dataset) constitute 44% of measurements.

The sensitivity of the model to its input parameters is determined in two stages. In the first stage, each of the input parameters is perturbed in turn by an amount corresponding to the estimated uncertainty in that parameter. Whilst each parameter is perturbed all other parameters remain at their default values (Knorr and Heimann, 2001). Default values (*def*) and parameter uncertainties (*uncert*) are taken from field measurements, and compilations thereof, given in Table 1. Eq. (5) yields χ^2 at (*def* + *uncert*) and (*def* − *uncert*). We use the average absolute change with respect to the unperturbed state, $\Delta(\chi^2)$, as a measure of model sensitivity to that parameter.

In the second stage, the most influential parameters are examined more closely. For each PFT, the nine most influential parameters determined from the first stage are perturbed as previously but now the remaining fixed parameters are assigned random values between their lower (*def* − *uncert*) and upper (*def* + *uncert*) limits. For 50 random realisations of the default configuration, mean $\Delta(\chi^2)$ and its standard deviation define model sensitivity for each influential parameter. This Monte Carlo approach reduces the dependence of the final parameter ranking on the default parameter configuration chosen in the first stage (Zaehle et al., 2005). The number of random realisations is necessarily small owing to the large number of measurements ($\simeq$ 1 million) compared against each simulation. However, when examining the limitations of our methodolgy (Section 3.3) we check the influence of the parameter ranking on the main results.

(2) Model optimisation and evaluation

Optimisation is conducted for each PFT separately by tuning the most influential parameters identified in the sensitivity analysis of part (1). In the past, up to 12 parameters have been fitted by comparing against observed fluxes (Friend et al., 2007). However, both Wang et al. (2001) and Medlyn et al. (2005) caution that a maximum of about 3–4 parameters can be reasonably constrained owing to dependencies between both input parameters and observed fluxes. To monitor the fitting process, this study increases the number of free (tuneable) parameters from 1 (the most influential found in the sensitivity analysis) up to a maximum of 7. Optimisation is achieved through the minimisation of χ^2 (Eq. (5)) using a Levenberg–Marquardt (LM) optimisation (Draper and Smith, 1981; Press et al., 1992). Each time the number of tuneable parameters is increased we check the covariance matrix produced by the optimisation algorithm. If the relative difference between the two largest elements of any eigenvector exceeds 1/3, the new parameter is rejected as this indicates a significant level of covariance between two parameters. Rejected parameters are replaced by the next most influential parameter until all 9 of the most influential parameters have been examined or the number of calibration parameters reaches 7. This procedure for the identifiability of parameters is similar to Wang et al. (2001) and Medlyn et al. (2005). It ensures sufficient degrees of freedom to allow the model to reproduce the observed fluxes whilst reducing redundancy in the tuning parameter set. Since the number of parameters chosen for tuning may differ between the two models we check the influence of the number of parameters on our main results.

The robustness of the LM-optimisation is tested by randomising the initial values of both fixed and tuneable parameters assuming a uniform probability density function between the parameter lower (*def* − *uncert*) and upper (*def* + *uncert*) limits. The standard deviation of the optimised value yields the uncertainty in the retrieval (Reichstein et al., 2003; Friend et al., 2007). We are aware that a diversity of methods are applied to the problem of model optimisation, including techniques for identifying the subsets of parameters which are retrievable (Medlyn et al., 2005). The approach adopted in the present investigation is well suited to the large number of parameters contained in the model (30-40) and the massive quantity of measured fluxes available for comparison.

Model performance at site-level is evaluated by comparing output from the optimised model with the observed fluxes over a range of timescales (half-hourly, daily and seasonal for JULES-SF and daily and seasonal for JULES-PEM). Our statistical analysis comprises the standard statistics adopted recently by land-surface modellers (e.g. Yuan et al., 2007; Fisher et al., 2008) as well as the Modelling Efficiency (MEF) which is similar to the coefficient of determination (r^2) but takes account of model bias (Medlyn et al., 2003):

$$\mathrm{MEF} = 1 - \frac{\sum (F_{sim} - F_{obs})^2}{\sum (F_{obs} - \langle F_{obs} \rangle)^2} \tag{6}$$

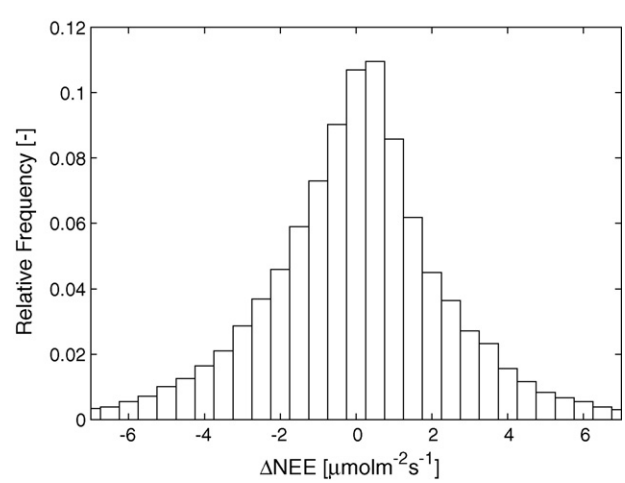

Fig. 1. Distribution of errors estimated for half-hourly Net Ecosystem Exchange (NEE) using the data bins described in Section 2.3. Δ NEE represents the distance from the corresponding bin average ($n = 154,000$). Results are only shown for needleleaf site-years which are the most numerous within the Marconi archive. For other plant functional types, the flux distribution, including that for latent heat, sensible heat and net radiation, is qualitatively similar.

Table 5
Optimised values for the most influential parameters according to model and Plant Functional Type (PFT). Models are JULES-SF (SF) and JULES-PEM (PEM). Plant Functional Types (PFTs) are designated as in Table 3. The standard deviation, in parentheses, derives from 50 random configurations of the initial parameter values (Section 2.3). Parameter symbols (given below each optimised value) and their units are defined in Table 1. Parameters having greatest influence over the optimisation fit are towards the left of the table.

Model	PFT	Parameter (decreasing influence →)				
		1	2	3	4	5
SF	BL	0.0018(0.0010)	36(16)	0.38(0.27)	47(7)	6.8(1.7)
		F_d	N_{eff}	k_{rub}	T_h	m
SF	NL	0.0099(0.0046)	3.5(1.9)	0.14(0.04)	0.0053(0.0014)	>20(3)
		F_d	m	T_{NIR}	dcatch0	$z1_u$
SF	C_3	0.0077(0.0032)	39(24)	18(5)	0.45(0.02)	–
		F_d	N_{eff}	m	T_{NIR}	–
SF	C_4	11(15)	0.019(0.005)	42(7)	3.2(0.8)	0.00(0.01)
		N_{eff}	QE	T_h	LAI	R_{grow}
SF	SH	12(5)	0.34(0.05)	0.0012(0.0004)	–	–
		N_{eff}	a_g	dz_m	–	–
SF	MX	12(8)	0.0085(0.0032)	11(14)	0.93(0.83)	–
		N_{eff}	F_d	T_l	Q_{10}(leaf	–
PEM	BL	0.31(0.09)	0.40(0.15)	−15(4)	–	–
		albnir	CUE	T_l	–	–
PEM	NL	0.20(0.09)	15(6)	4.1(1.1)	–	–
		albnir	c_i	$z1_u$	–	–
PEM	C_3	0.44(0.09)	0.34(0.15)	14(5)	7.4(1.2)	–
		albnir	CUE	c_i	b	
PEM	C_4	0.29(0.09)	0.32(0.17)	2.6(0.7)	4.6(1.2)	13(6)
		albnir	CUE	$z1_u$	b	c_i
PEM	SH	0.34(0.09)	4.0(1.4)	−15(18)	0.39(0.07)	–
		albnir	$z1_u$	T_l	SMCV	–
PEM	MX	0.09(0.09)	0.14(0.09)	3.0(1.2)	1.7e −8(0.1e −8)	–
		albnir	CUE	ϵ	κ	–

where $\langle F_{obs} \rangle$ is the mean of the observations. The statistical distribution underlying eddy covariance is poorly known although ΔF_{obs} estimated for Eq. (5) suggests an imperfect gaussian distribution which is nonetheless symmetric (Fig. 1). Therefore, we also compute the non-parametric Spearman's rank correlation coefficient (Norcliffe, 1977).

3. Results

3.1. Sensitivity analysis and model optimisation

Both models are sensitive to parameters governing gross productivity and autotrophic respiration, especially photosynthetic

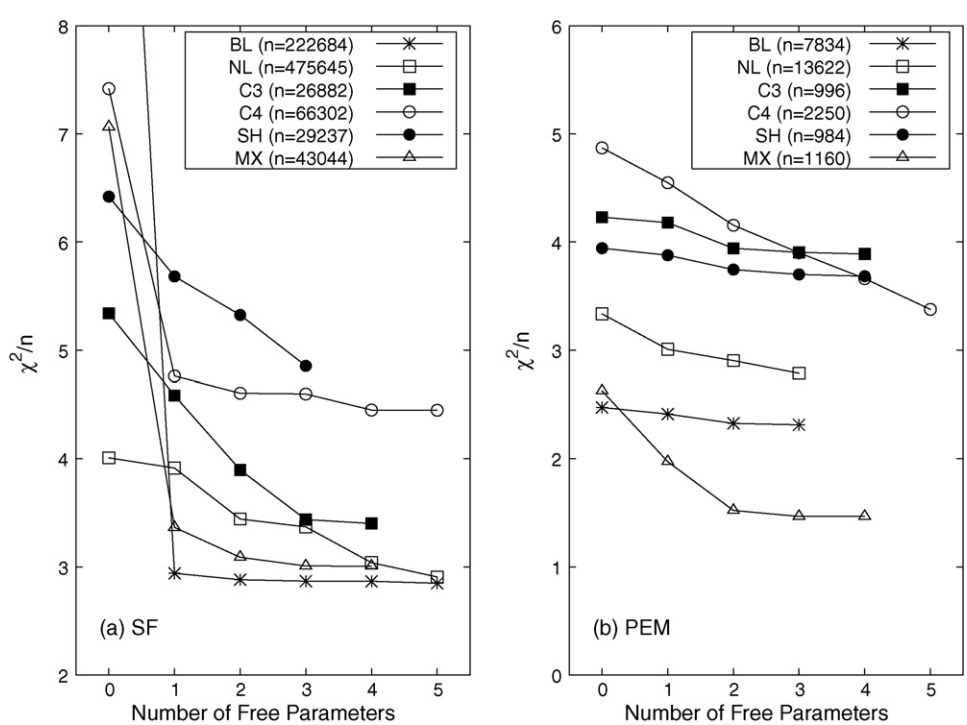

Fig. 2. Improvement in model fit as the number of free parameters is increased. For each PFT, the fit is given by χ^2 normalised by the number of measurements (n). χ^2 is calculated using half-hourly fluxes for JULES-SF (panel a) and daily fluxes for JULES-PEM (panel b). Note that χ^2/n is only indicative since we likely overestimate the random observational error, especially for JULES-PEM. PFTs are designated as in Table 3. For BL, χ^2/n=13.5 when no tuning parameters are used (zero free parameters).

capacity (N_{eff}) and leaf dark respiration (F_d) within JULES-SF, and *CUE* and ϵ within JULES-PEM (Table 5). The important role of photosynthetic capacity is already noted for several LSMs (Dang et al., 1998; Reichstein et al., 2003; Wang et al., 2001). In agreement with previous authors (Reichstein et al., 2003; Misson et al., 2004; Knorr and Kattge, 2005), parameters governing stomatal conductance are also found to be influential, i.e. m within JULES-SF and c_i within JULES-PEM. A third group of influential parameters emerge which govern shortwave energy balance and surface temperature (T_{NIR} and a_g in JULES-SF and *albnir* in JULES-PEM). It is particularly important to constrain properties in the near-infrared waveband (via T_{NIR} and *albnir*) which are known to diverge dramatically for photosynthetic and non-photosynthetic elements within the vegetation canopy. Leaves are fairly poorly absorbers of near-infrared radiation whilst trunks and branches are not (Williams, 1991).

In general, the three most influential parameters for each PFT and model lie within $\simeq 1\sigma$ of the literature values given in Table 1. Notable exceptions are (1) ground albedo (a_g) for shrubs which is rather high, possibly owing to snow cover at the beginning of the growing season; and (2) the lower inhibition temperature for leaf photosynthesis (T_l) which operates through an exponential relationship meaning that the model is relatively insensitive to the precise lower limit during the growing season once this limits fall below $\simeq -5^\circ$ C (furthermore, optimisation is limited to the growing season and temperatures during the growing season are generally well above T_l). The uncertainties in the optimised values are quite large owing to both site variation (discussed below) and covariance between tuning parameters. The latter is reduced, but not completely eliminated, by the parameter selection procedure adopted in Section 2.3. The parameter range for the PEM is also likely to be overestimated owing to the relatively large errors we assume for the daily observational fluxes (Section 2.3).

Fig. 2 reveals how χ^2 evolves as the number of free parameters adopted in the optimisation increases incrementally from 0 to the maximum number determined in the sensitivity analysis. The

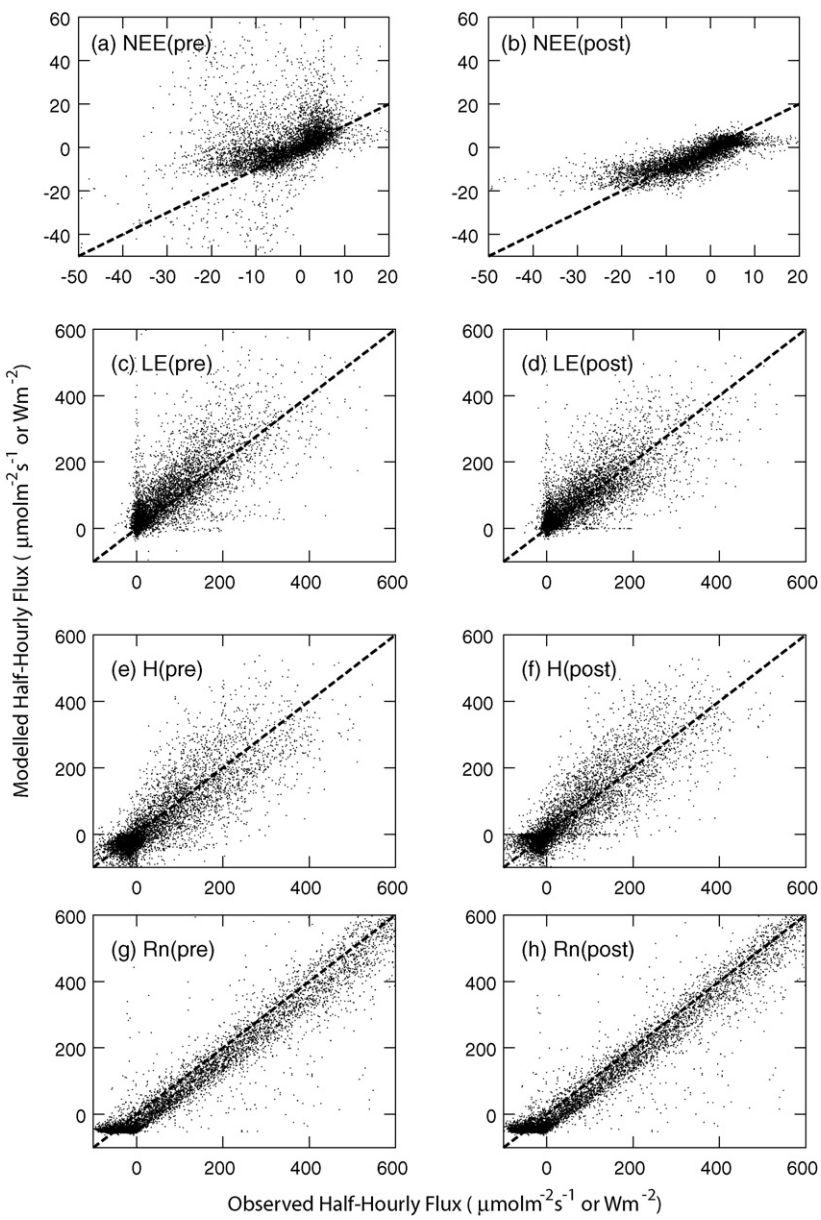

Fig. 3. Comparison of observed half-hourly fluxes against values simulated with JULES-SF. The quantities NEE, LE, H and Rn denote, respectively, Net Ecosystem Exchange (μ mol m^{-2} s^{-1}), latent heat flux (W m^{-2}), sensible heat flux (W m^{-2}) and net radiative exchange (W m^{-2}). A comparison is made both before (pre) and after (post) optimisation of the most influential parameters for each PFT. The dashed line denotes $y = x$.

Table 6
Regression and error analysis of half-hourly fluxes predicted by JULES-SF after model optimisation. Information is shown per Plant Functional Type (PFT) for Net Ecosystem Exchange (NEE), latent heat (LE), sensible heat (H) and net radiation (Rn). PFTs are designated as in Table 3. The following indices Janssen and Heuberger, 1995 are given: the number of fitted data (n); the modelling efficiency (MEF); gradient (a) and intercept (b) of a least-squares linear fit; the coefficient of determination (r^2); the mean absolute error (MAE); mean observed flux (⟨obs⟩); and the mean simulated flux (⟨mod⟩).

PFT	Flux	Units	n	MEF	a	b	r^2	MAE	⟨obs⟩	⟨mod⟩
BL	NEE	μ mol m^{-2} s^{-1}	59,184	0.71	0.65	−2.7	0.73	3.7	−5.1	−6.0
BL	LE	W m^{-2}	61,797	0.63	0.89	31	0.72	38	76	98
BL	H	W m^{-2}	53,113	0.63	0.98	6.5	0.72	41	47	53
BL	Rn	W m^{-2}	48,590	0.90	0.93	−16	0.91	42	180	150
NL	NEE	μ mol m^{-2} s^{-1}	109,250	0.60	0.55	−1.7	0.61	3.4	−2.7	−3.2
NL	LE	W m^{-2}	113,118	0.53	0.66	22	0.55	33	65	65
NL	H	W m^{-2}	116,862	0.72	0.91	12	0.75	41	63	70
NL	Rn	W m^{-2}	136,415	0.93	0.93	−8.2	0.94	39	160	140
C_3	NEE	μmol m^{-2} s^{-1}	6,174	0.57	0.53	−2.3	0.58	3.9	−3.6	−4.2
C_3	LE	W m^{-2}	5,557	0.78	0.93	12	0.80	40	130	130
C_3	H	W m^{-2}	6,534	0.43	0.89	3.5	0.59	36	34	34
C_3	Rn	W m^{-2}	8,617	0.96	1.0	−10	0.96	28	160	150
C_4	NEE	μ mol m^{-2} s^{-1}	13,793	0.41	0.36	−3.0	0.44	6.5	−6.6	−5.4
C_4	LE	W m^{-2}	12,987	0.56	1.1	15	0.76	48	120	140
C_4	H	W m^{-2}	13,388	0.68	0.95	13	0.75	32	59	70
C_4	Rn	W m^{-2}	14,684	0.98	1.1	-18	0.99	27	230	230
SH	NEE	μ mol m^{-2} s^{-1}	6,838	0.26	0.28	−0.70	0.26	1.2	−0.82	−0.93
SH	LE	W m^{-2}	6,818	0.47	0.86	−4.1	0.62	23	44	34
SH	H	W m^{-2}	6,867	0.35	0.77	6.0	0.50	29	46	42
SH	Rn	W m^{-2}	8,714	0.77	0.98	-35	0.88	49	110	71
MX	NEE	μ mol m^{-2} s^{-1}	10,633	0.68	0.80	−0.58	0.69	2.8	−1.4	−1.7
MX	LE	W m^{-2}	11,580	0.52	0.65	40	0.57	43	63	81
MX	H	W m^{-2}	11,625	0.18	1.1	−4.2	0.62	43	26	26
MX	Rn	W m^{-2}	9,206	0.95	0.95	−20	0.97	36	160	130

general convergence in χ^2 suggests that a limited number of parameters can be optimised since, adding further parameters, improves the fit only marginally. The required number of parameters for convergence varies somewhat between PFTs but 3–4 appears to suffice in most cases. A similar conclusion is drawn from fluxes recorded at individual sites using a diversity of optimisation methods (Wang et al., 2001; Medlyn et al., 2003; Knorr and Kattge, 2005). The present investigation, by examining fluxes from 30 sites using both a simple and a complex LSM, tends to generalise the inference that the amount of biophysical information that can be retrieved from four observables (NEE, LE, H and Rn) is quite limited. It is possible that further parameters can be retrieved by examining sites individually. However, it is not clear to what extent such parameter values, based on a single site, are valid in a global model. A good model fit formally requires $\chi^2/n \simeq 1$ (Draper and Smith, 1981; Press et al., 1992). However, our values of χ^2/n in Fig. 2 are purely indicative and cannot be used to compare the performance of the two models.

3.2. Model evaluation

After optimisation, there is a significant improvement in the half-hourly fluxes predicted by JULES-SF (Fig. 3). Without tuning (i.e. using literature parameter values) the model performance is fairly poor for NEE. This is particularly true for broadleaf and mixed forest where autotrophic respiration is greatly over-estimated and the tuning of the most influential parameter F_d (leaf dark respiration) produces a rapid decrease in χ^2. The modelling efficiency of the optimised model is greatest for Rn (0.90–0.98) and least for NEE (0.26–0.71; Table 6). Model performance is poorer towards minimum and maximum observed NEE. As discussed below, this is mainly due to the calibration of the model at PFT-level as opposed to a separate tuning to individual sites. For JULES-PEM, the improvement in model performance is less dramatic after optimisation (Fig. 4). This is particularly true for carbon exchange, where a large amount of scatter remains after tuning. A complete residual analysis is beyond the scope of the current investigation but JULES-PEM appears to be severely limited in its ability to predict NEE over the full range of daily shortwave irradiance (Fig. 5). Furthermore, daily variability in the difference between autotrophic respiration and gross productivity is poorly captured by JULES-PEM since this difference is determined by a single parameter *CUE*. Optimised values of *CUE* are typically 0.3–0.4 and this tends to preclude modelled NEE greatly exceeding 0 unless soil respiration is very high (Fig. 4).

After optimisation, JULES-SF performs better than JULES-PEM on both daily (Table 7) and seasonal (Table 8) timescales. This is despite tuning a similar number of free parameters in each model. However, the difference in model performance appears to diminish with an increase in measurement timescale. Thus, on average, the modelling efficiency increases from 0.32 (daily) to 0.46 (seasonal) using the PEM approach, whilst it remains close to 0.6 for JULES-SF on both timescales. The non-parametric Spearman's rank correlation coefficient exhibits a similar convergent behaviour. The coefficient of determination (r^2), although it does not take account of bias, shows an even greater convergence, increasing on average from 0.53 (daily) to 0.71 (seasonal) for JULES-PEM but only from 0.69 to 0.75 for JULES-SF. Overall, the mean observed fluxes are predicted within, respectively, $\simeq$10% and $\simeq$20% for JULES-SF and JULES-PEM.

3.3. Caveats and limitations

The limitations of the methodology are examined within the context of the main finding, i.e. that JULES-SF performs better than JULES-PEM on all temporal scales:

1. We test the impact of the number of tuning parameters, which differs slightly between JULES-PEM and JULES-SF, by simply tuning the seven most influential parameters for each PFT, i.e. without rejection of covariant parameters. As previously, JULES-

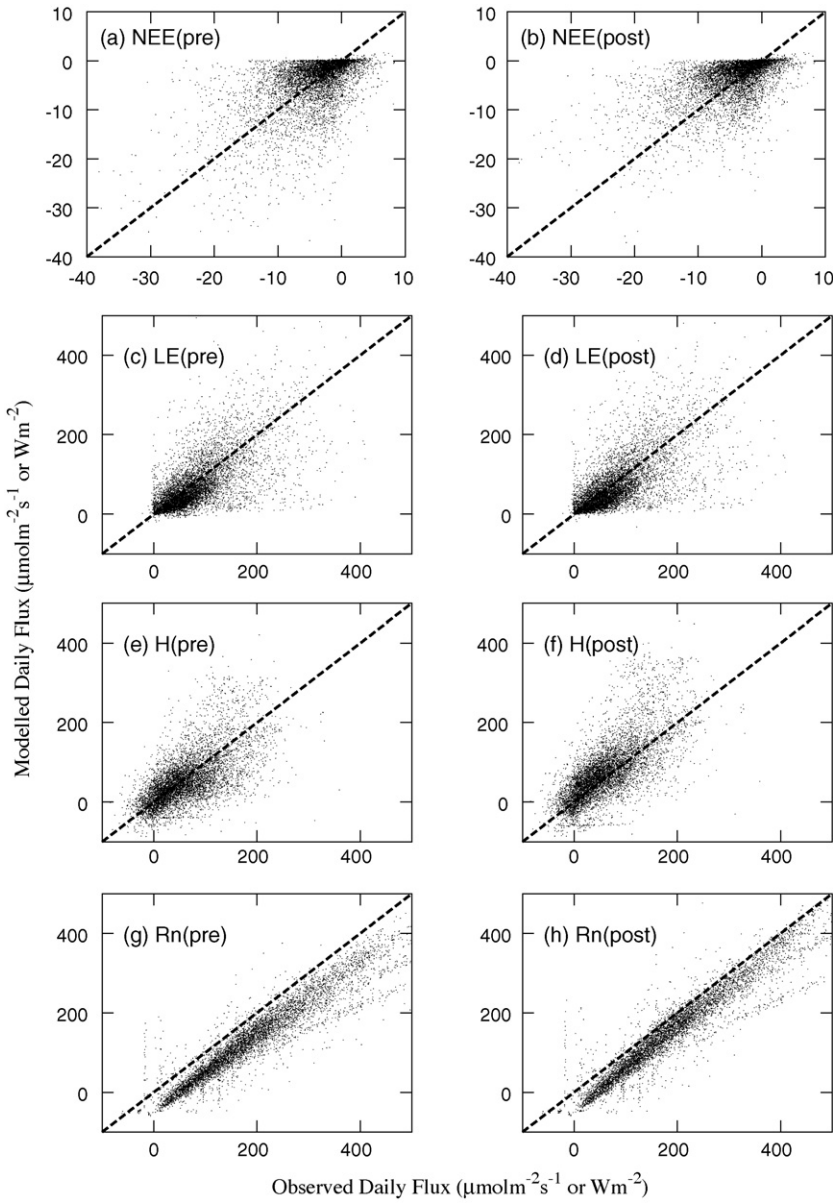

Fig. 4. As Fig. 3 but comparing average daily observed fluxes with output from JULES-PEM. For the purposes of comparison the same units are retained as Fig. 3.

SF performs better than JULES-PEM on all timescales and the difference in model performance diminishes with an increase in measurement timescale. Thus, r^2 increases from 0.76 (daily) to 0.84 (seasonal) for JULES-SF and from 0.63 (daily) to 0.84 (seasonal) for JULES-PEM ($p < 0.01$). This test also indicates that our main result is not too sensitive to the exact parameter ranking derived in the sensitivity analysis (Section 2.3) since a maximum number of tuneable parameters (7) produces a similar result to a more restricted number of free parameters (3–5). The ranking of parameters is only accurate to within 1–2 (Table 9).

2. To assess the impact of site variation within the same PFT, the most influential parameters are tuned separately for each site. The main result is unchanged by this procedure. Thus, r^2 increases from 0.75 (daily) to 0.84 (seasonal) for JULES-SF and from 0.56 (daily) to 0.79 (seasonal) for JULES-PEM ($p < 0.01$). Separate tuning of the model to individual sites improves the reproduction of observed site-level fluxes (Fig. 6), suggesting some variation between sites comprising the same PFT.
3. It is desirable to use separate sites for the purposes of calibration and validation. However, the paucity of site-years, particularly for shrubs and grasses, necessitates the pooling of data to provide a robust calibration. To test the impact of this aggregation, half the FLUXNET sites are randomly selected for parameter optimisation and the remaining sites are used for the comparison of model performance. As previously, JULES-SF performs better than JULES-PEM on all timescales and the difference in model performance diminishes with increasing timescale. Thus, r^2 increases from 0.70 (daily) to 0.74 (seasonal) for JULES-SF and from 0.55 (daily) to 0.74 (seasonal) for JULES-PEM ($p < 0.01$). The modelling efficiency increases from 0.22 (daily) to 0.38 (seasonal) using the PEM approach, whilst it falls slightly from 0.59 to 0.55 using JULES-SF.
4. Hollinger and Richardson (2005) recommend a cost function based on absolute deviation, rather than square deviation, when calibrating against eddy covariance fluxes since observational errors exhibit a double exponential rather than gaussian

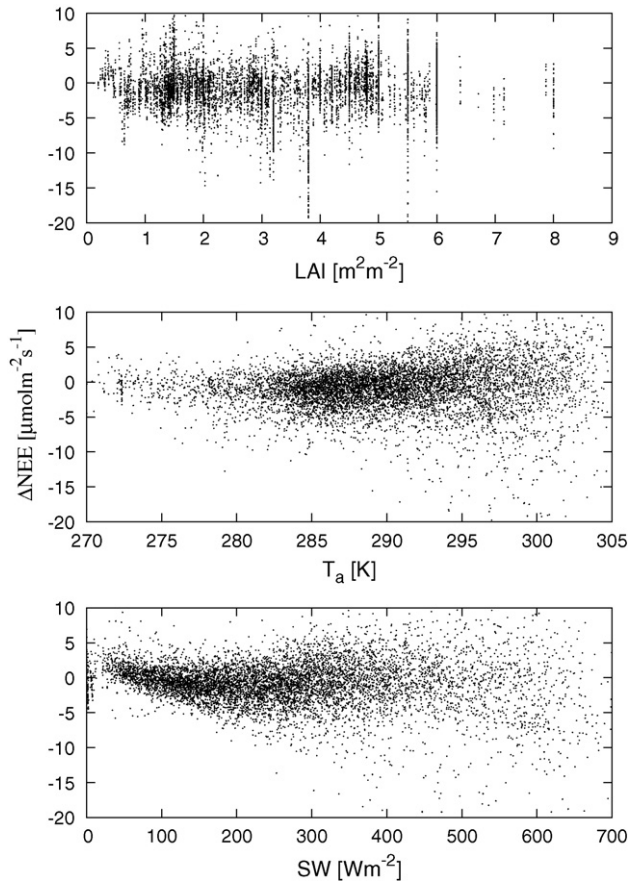

Fig. 5. Observed minus simulated values of daily averaged Net Ecosystem Exchange (ΔNEE). Simulated values are from JULES-PEM after model optimisation. A comparison is made against daily averages of solar irradiance (SW), air temperature (T_a) and leaf area index (LAI).

distribution. If we make this modification to Eq. (5), the optimal parameter values are not changed significantly.

4. Discussion

After optimisation, the complex process-based LSM, with its multilayer representation of light interception and canopy properties (JULES-SF), performs better than a productivity efficiency approach (JULES-PEM) at all temporal scales. This conclusion appears to be more or less independent of the precise manner in which the LSM is calibrated. However, the difference in model performance is reduced when comparing over larger (seasonal) timescales. This convergence between the two modelling approaches is noted by Medlyn et al. (2003) who compare a sun-shade model, of comparable complexity to JULES-SF, with a PEM. Canopy GPP at a single needleleaf site is used for validation in this case. The error in the PEM falls from $\simeq$25% on daily timescales to $\simeq$15% on monthly timescales whilst the error in the sun-shade model (10–15%) is fairly constant over both timescales.

We might expect the multilayer LSM to perform better than the PEM approach owing to the complexity of the former. However, more explicit representations of land-surface processes require more parameters. Some of these parameters are poorly measured or unavailable from field measurements. Furthermore, the present investigation, as well as several previous studies (Wang et al., 2001; Medlyn et al., 2003; Knorr and Kattge, 2005), suggest that a fairly limited number of parameters can be optimised on the basis of a small number of observables. Under such circumstances, increasing the number of irretrievable parameters within the model may actually increase the 'noise' within the calculation. In any case, it is instructive to compare the accuracy provided by each method. Whilst a multilayer, process-based approach is being adopted increasingly in several global LSMs (e.g. Dai et al., 2004; Alton et al., 2007b), the PEM-approach is still used extensively on various spatial scales (Potter et al., 1993; Goetz and Prince, 1996; Barrett, 2002; Medlyn et al., 2003; Yuan et al., 2007), including the derivation of daily global GPP from MODIS satellite data (Running et al., 2004; Zhao et al., 2005; Heinsch et al., 2006).

Table 7
Error and regressional analysis of daily fluxes after optimisation of JULES-SF (SF) and JULES-PEM (PEM). Statistical indices (defined in Table 6) combine all site-years and are calculated per flux. The Spearman's rank correlation coefficient Norcliffe, 1977 is denoted by r_s. Energy fluxes are given in mm of water per day assuming a latent heat evaporation of 43 kJ mol^{-1}.

Model	Flux	Units	n	MEF	a	b	r^2	MAE	⟨obs⟩	⟨mod⟩	r_s
SF	NEE	kg m^{-2} day^{-1}	6759	0.56	0.51	−0.0024	0.57	0.0025	−0.0045	−0.0047	0.76
SF	LE	mm day^{-1}	6972	0.49	0.82	0.85	0.60	1.1	2.9	3.2	0.78
SF	H	mm day^{-1}	6784	0.47	1.0	0.26	0.67	1.1	2.1	2.4	0.85
SF	Rn	mm day^{-1}	6449	0.86	1.0	−0.78	0.90	1.1	6.5	5.8	0.96
PEM	NEE	kg m^{-2} day^{-1}	6729	0.21	0.44	−0.0018	0.30	0.0034	−0.0045	−0.0038	0.54
PEM	LE	mm day^{-1}	6941	0.21	0.71	0.48	0.43	1.3	2.9	2.5	0.68
PEM	H	mm day^{-1}	6756	0.08	0.91	0.69	0.50	1.4	2.2	2.7	0.73
PEM	Rn	mm day^{-1}	6420	0.79	0.94	−0.92	0.90	1.5	6.6	5.2	0.95

Table 8
As Table 7 but comparing fluxes integrated over the entire growing season.

Model	Flux	Units	n	MEF	a	b	r^2	MAE	⟨obs⟩	⟨mod⟩	r_s
SF	NEE	kg m^{-2} season^{-1}	71	0.67	0.63	−0.18	0.67	0.15	−0.43	−0.45	0.87
SF	LE	mm season^{-1}	71	0.61	0.85	76	0.69	77	280	320	0.89
SF	H	mm season^{-1}	68	0.30	1.2	−12	0.70	73	210	240	0.84
SF	Rn	mm season^{-1}	56	0.86	1.0	−75	0.92	90	750	670	0.97
PEM	NEE	kg m^{-2} season^{-1}	71	0.56	0.56	−0.12	0.59	0.18	−0.43	−0.36	0.72
PEM	LE	mm season^{-1}	71	0.61	0.67	59	0.65	68	280	250	0.85
PEM	H	mm season^{-1}	68	−0.01	1.2	−2.9	0.66	91	210	260	0.77
PEM	Rn	mm season^{-1}	56	0.71	0.91	−83	0.92	150	750	600	0.97

Table 9
The most influential parameters per Plant Functional Type (PFT) per model, determined as identifiable in the sensitivity analysis. The ranking is determined by the mean value of $\Delta(\chi^2)/n$ (in parentheses) from over 50 random realisations of the default parameter configuration (Section 2.3). PFTs are designated as in Table 3.

Model	Rank	BL	NL	C_3	C_4	SH	MX
SF	1	F_d (26±5.1)	F_d (0.51 ±0.10)	F_d (1.2 ±0.28)	N_{eff} (2.1 ±0.18)	N_{eff} (0.55 ±0.08)	N_{eff} (9.8 ±1.3)
SF	2	N_{eff} (25 ±3.8)	m (0.34 ±0.03)	N_{eff} (1.1 ±0.28)	QE (1.3 ±0.21)	a_g (0.32 ±0.01)	F_d (7.3 ±1.2)
SF	3	k_{rub} (12 ±3.0)	T_{NIR} (0.31 ±0.02)	m (1.0 ±0.13)	T_h (1.3 ±0.14)	dz_m (0.27 ±0.01)	T_l (1.8 ±0.32)
SF	4	T_h (8.9 ±1.9)	dcatch0 (0.28 ±0.02)	T_{NIR} (0.70 ±0.04)	LAI_{max} (1.0 ±0.09)		Q_{10}(leaf) (1.4 ±0.22)
SF	5	m (5.3 ±0.9)	$z1_u$ (0.24 ±0.01)		R_{grow} (0.91 ±0.12)		
PEM	1	albnir (1.1 ±0.0)	albnir (1.4 ±0.0)	albnir (2.4 ±0.0)	albnir (5.0 ±0.0)	albnir (1.6 ±0.0)	albnir (1.3 ±0.0)
PEM	2	CUE (0.30 ±0.01)	c_i (0.11 ±0.0)	CUE (0.27 ±0.01)	CUE (0.52 ±0.03)	$z1_u$ (0.098 ±0.003)	CUE (0.44 ±0.04)
PEM	3	T_l (0.081 ±0.003)	$z1_u$ (0.067 ±0.003)	c_i (0.23 ±0.01)	$z1_u$ (0.34 ±0.02)	T_l (0.068 ±0.003)	ϵ (0.33 ±0.03)
PEM	4			b (0.19 ±0.01)	b (0.34 ±0.02)	SMCV (0.034 ±0.002)	κ (0.069 ±0.006)
PEM	5				c_i (0.15 ±0.01)		

Friend et al. (1997) question the merit of tuning LSMs since the number of degrees of freedom within such models is large. On the basis of our results we feel, however, that there is an inherent assumption in this assertion that land-surface processes are sufficiently well represented to allow the LSM to reproduce the observations at all timesteps. For the daily PEM, used in the current investigation, this does not appear to be the case (Fig. 4). It also assumes that model tuning is temporally scale-invariant. The change in model performance by JULES-PEM at longer timescales suggests that this might not be true, as discussed below. Friend et al. (1997) advocate the use of field measurements from the literature when calibrating an LSM. Whilst this approach is desirable, literature values for several key parameters are highly uncertain (Table 1). Thus, even complex models, such as JULES-SF, have difficulty reproducing observed fluxes without some prior tuning (Fig. 3). This limitation is also recognised by Zaehle et al. (2005) when examining the performance of the Lund-Potsdam-Jena (LPJ) model. The relatively weak performance of JULES-PEM on daily timescales, even after parameter tuning (Fig. 4), suggests that complex models, such as JULES-SF, may benefit more from site-level calibrations compared to simpler models. Indeed, Abramowitz et al. (2007) argue that model bias is the dominant error in land-surface modelling and the improved representation of biophysical processes should be the first priority rather than parameter optimisation. When supplied with the same input, LSMs produce values of global NPP which deviate by ±20% from the mean (Cramer et al., 2001). Thus, the complexity with which land-surface processes should be represented in global LSMs is clearly important (Knorr and Heimann, 2001).

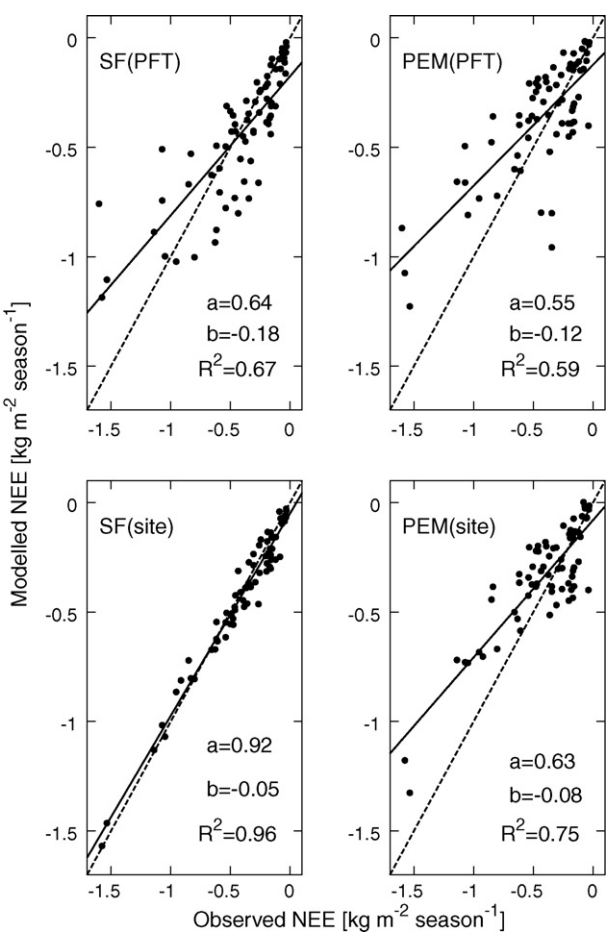

Fig. 6. Modelled versus observed Net Ecosystem Exchange (NEE) for 71 site-years (30 sites), integrated over the growing season. JULES-SF (SF) and JULES-PEM (PEM) are either calibrated per Plant Functional Type (denoted PFT) or per individual location (denoted site). Solid and dashed lines represent, respectively, the linear best fit ($y = ax + b$) and $y = x$. For all best fits $p < 0.01$.

Despite its somewhat weaker performance, the PEM possesses a number of advantages over a more process-based, complex approach. We are required to specify 38 input parameters for JULES-SF but only 28 for JULES-PEM. In the absence of canopy structure, and by virtue of a longer timestep, computational times are an order of magnitude smaller with the PEM. This is an important consideration when conducting global simulations over decadal/century timescales or when near real-time global fluxes are required as in the MODIS algorithm. The strong correlation observed between instantaneous midday and daily average LUE (GPP/APAR) at FLUXNET sites (Sims et al., 2005) also appears to justify the use of linear relationships for canopy photosynthesis. However, observed NEE appears to possess a more complicated relationship with respect to incident sunlight. The large residuals with respect to shortwave radiation (Fig. 5) might be explained by the small magnitude of NEE relative to GPP. Since NEE reflects a fine balance between gross productivity and respiration, small inaccuracies in predicted GPP may have a dramatic effect on modelled NEE.

The manner in which PEMs are calibrated appears to play a key role in their usefulness. For example, weekly averaged LUE possesses a regressional slope against instantaneous midday LUE which is significantly different from unity (Sims et al., 2005). This suggests that a PEM approach is useful so long as the corresponding potential LUE (parameter ϵ) is adjusted according to the timescale of the observation. There is some evidence to suggest that the PEM-approach is best applied on timescales of 2 weeks or more (Medlyn et al., 2003). Indeed, our own results are consistent with that conclusion. However, even on daily timescales, the PEM reproduces site-level GPP within 20–30% (Medlyn et al., 2003; Heinsch et al., 2006; Yuan et al., 2007). Indeed, global GPP is derived on this timescale with MODIS (Running et al., 2004). The MODIS algorithm is notable in that, prior to satellite launch, a more

complex, process-based LSM (BIOME-BGC) was used to calibrate the PEM algorithm for each PFT (Zhao et al., 2005).

5. Conclusions

We compare the performance of a productivity efficiency model (JULES-PEM) with a more complex, multilayer model that has recently been enhanced to take account of sunfleck penetration and diffuse sunlight (JULES-SF). JULES-PEM contains no canopy structure and is based on daily LUE. JULES-SF is driven by half-hourly climate at site-level and takes account of changes in leaf nitrogen, microclimate and light interception with depth through the canopy. Optimisation of both models is conducted against observed fluxes (NEE, LE, H and Rn) from 30 FLUXNET sites spanning a wide range of PFTs (71 site-years in all). Our main conclusions are as follows:

1. The process-based, multilayer model performs better than a productivity efficiency approach. However, the difference in model performance appears to diminish with an increase in measurement timescale. Thus, on average, the modelling efficiency increases from 0.32 (daily) to 0.46 (seasonal) using the PEM approach, whilst it remains close to 0.6 for JULES-SF on both timescales. Both the coefficient of determination (r^2) and the non-parametric Spearman's rank correlation coefficient demonstrate a similar convergence in model performance. Overall, the mean observed fluxes are predicted within, respectively, $\simeq$10% and $\simeq$20% using JULES-SF and JULES-PEM.
2. For any given PFT, the maximum number of biophysical parameters that can be tuned against four observables (NEE, LE, H and Rn) is quite limited (3–4). This is true for both models despite their considerable difference in complexity.

Acknowledgements

We are grateful to the PIs and Co-Is of FLUXNET who make their data freely available to the ecological modelling community through the Marconi archive, namely: E. Falge, M. Aubinet, P. Bakwin, P. Berbigier, C. Bernhofer, A. Black, R. Ceulemans, A. Dolman, A. Goldstein, M. Goulden, A. Granier, D. Hollinger, P. Jarvis, N. Jensen, K. Pilegaard, G. Katul, P. Kyaw Tha Paw, B. Law, A. Lindroth, D. Loustau, Y. Mahli, R. Manson, P.Moncrieff, E. Moors, W. Munger, T. Meyers, W. Oechel, E. Schulze, H. Thorgeirsson, J. Tenhunen, R. Valentini, S. Verma, T. Vesala, and S. Wofsy. 2005. FLUXNET Marconi Conference Gap-Filled Flux and Meteorology Data (1992–2000) are available online from Oak Ridge National Laboratory Distributed Active Archive Center http://www.daac.ornl.gov. This work is supported by the Natural Environment Research Council (NERC) under grant NE/F00205X/1.

Appendix A. Description of JULES-SF

The Joint UK Land Environmental Simulator (JULES) is forced by the following meteorological variables: downwelling shortwave radiation, downwelling longwave radiation, precipitation, air temperature, windspeed, air humidity and pressure. The energy calculation central to the model is based on a Penman–Monteith approach (Monteith, 1965), ensuring that the downwelling shortwave and longwave fluxes are balanced by the outgoing fluxes of sensible heat, latent heat, reflected shortwave radiation, radiant thermal energy and conduction into the ground. Surface albedo and the penetration of light into the canopy are estimated according to the two-stream formulation (Sellers et al., 1996a). Stomatal conductance, leaf boundary-layer resistance, transpiration and photosynthesis are calculated in each canopy layer, before summing to produce total values for the entire canopy (Alton et al., 2007a; Mercado et al., 2007). In general, five layers provide sufficient numerical precision and we adopt this number for the current study.

Alton et al. (2007a) enhance the standard JULES version to take account of sunfleck penetration, explicit leaf orientation and diffuse sunlight. This modification (JULES-SF) produces a more realistic canopy response under both direct sunlight and cloud (Alton et al., 2005, 2007a). A sunfleck reaches a given canopy layer if a randomly generated number, between 0 and 1, is less than or equal to P, where:

$$P = \exp\left(\frac{-LAI_c \times k_{ext}}{\cos(\theta_s)}\right) \tag{7}$$

and LAI_c is the cumulative LAI lying above the leaf layer, θ_s is the solar zenith angle and k_{ext} is the light extinction coefficient (Norman, 1981; Jones, 1992). Assuming a spherical Leaf Angle Distribution (Campbell and Norman, 1998), k_{ext} = 0.5. Diffuse light in the canopy follows from the two-stream formulation, the equations for which are given by (Sellers et al., 1996a). At any given timestep, the fraction of diffuse sunlight incident at the top of the canopy is derived using the ratio of observed surface irradiance and top-of-atmosphere irradiance, as given by (Roderick et al., 2001).

Leaf photosynthesis for the C_3 and C_4 pathways are derived using the co-limitation model of (Collatz et al., 1991, 1992) which is conceptually similar to the biochemical model of Farquhar et al. (1980). The leaf photosynthetic rate A_l (μ mol m^{-2} s^{-1}) is the smoothed minimum of three limits: the photosynthetic rate due to incident light J_{PAR}; photosynthetic capacity due to the concentration and chemical activity of ribulose-1,5-bisphosphate carboxylase/oxygenase (i.e. Rubisco) J_r; and the photosynthetic rate based on the ability of the leaf to export the products of photosynthesis J_e. Four of the five Plant Functional Types defined in JULES concern the C_3 pathway and we elaborate the corresponding equations below. Note, however, that these leaf photosynthetic limits (Eqs. (8), (9) and (11)) change somewhat for the C_4 pathway as detailed in Collatz et al. (1992) and Sellers et al. (1996b).

The light-limited rate is given thus:

$$J_{PAR} = QE \times I_L \times \frac{c_i - c_0}{c_i + 2 \times c_0} \tag{8}$$

where QE is the quantum efficiency and I_L (μ mol m^{-2} s^{-1}) is the leaf PAR irradiance. c_i (mol mol^{-1}) and c_0 (mol mol^{-1}) are, respectively, the CO_2 concentration internal to the leaf and the photorespiratory compensatory point.

The Rubisco-limited rate of leaf photosynthesis is given by:

$$J_r = \frac{V_m \times (c_i - c_0)}{c_i + K_c(1 + O_a/K_o)} \tag{9}$$

where K_c (mol mol^{-1}) and K_o (mol mol^{-1}) are the Michaelis constants determining the competing rates of carboxylation and oxgenation and O_a is the oxygen concentration (mol mol^{-1}). V_m (μ mol m^{-2} s^{-1}) describes the chemical activity of Rubisco at leaf temperature T_L (°C):

$$V_m = \frac{V_{cmax} \times Q_{10}^{0.1(T_L-25)}}{(1 + e^{0.3(T_L-T_h)}) \times (1 + e^{0.3(T_l-T_L)})} \tag{10}$$

where Q_{10} is a dimensionless coefficient for leaf respiration. T_l and T_h are the inhibition temperatures (°C) for photosynthesis. Thus, the ratio V_m/ V_{cmax} (= FT) can be considered as the stress on photosynthesis owing to temperature. V_{cmax} is the leaf photosynthetic capacity at the top of the canopy. Both V_{cmax} and QE decline exponentially according to the nitrogen allocation coefficient k_{rub} and cumulative LAI (Hirose and Werger, 1987).

Finally, the export-limited rate of leaf photosynthesis is determined by:

$$J_e = \frac{V_m}{2} \tag{11}$$

Leaf respiration R_L is set to $0.015 \times V_m$ (Collatz et al., 1991). Total plant respiration (R_P) consists of respiration for maintenance (R_{PM}) and for growth (R_{PG}). The former scales as the plant-to-leaf nitrogen ratio (PL):

$$R_{PM} = PL \times R_L \tag{12}$$

Growth respiration is a prescribed fraction (R_{grow}) of the difference between gross productivity and maintenance respiration (Ryan, 1991b):

$$R_{PG} = R_{grow} \times (GPP - R_{PM}) \tag{13}$$

Leaf stomatal conductance (g_l; mol m^{-2} s^{-1}) within each leaf layer is calculated according to the Ball–Berry relation:

$$g_l = m \times \frac{A_l H}{c_i} + g_{\min} \tag{14}$$

where A_l is the leaf photosynthetic rate (mol m^{-2} s^{-1}), H is the relative humidity of the canopy airspace, m the stomatal slope factor, and $g_{\min}$ (mol m^{-2} s^{-1}) is the minimum stomatal conductance (Ball et al., 1987; Collatz et al., 1991, 1992; Sellers et al., 1996b). The stomatal parameters (m and g_{min}) assume different values for the C_3 and C_4 pathways (Collatz et al., 1991, 1992).

Rubisco-limited photosynthetic capacity, leaf respiration and g_{min} are all linearly dependent on the soil moisture factor (FSMC). FSMC depends exponentially on soil water potential, ψ_s (MPa):

$$FSMC = \frac{1}{1 + \exp(2(\psi_c - \psi_s))} \tag{15}$$

where ψ_c is the critical soil water potential (Sellers et al., 1996b). Eq. (15) is consistent with the steep rise in rhizospheric hydraulic resistance observed at low soil moisture content (Newman, 1969) and differs from the JULES standard release which utilises a linear ramp function for FSMC.

For further explanation concerning the role of the original JULES parameters we refer to Cox et al. (1999) and Cox (2001).

References

Abramowitz, G., Pitman, A., Gupta, H., Kowalczyk, E., Wang, Y.-P., 2007. Systematic bias in land surface models. Journal of Hydrometeorology 8, 989–1001.

Al-Khatib, K., Paulsen, G., 1999. High-temperature effects on photosynthetic processes in temperate and tropical cereals. Crop Science 39, 119–125.

Alton, P., North, P., Kaduk, J., Los, S., 2005. Radiative transfer modelling of direct and diffuse sunlight in a siberian pine forest. JGR Atmospheres 110, 23209.

Alton, P., North, P., Los, S., 2007a. The impact of diffuse sunlight on canopy light-use efficiency, gross photosynthetic product and net ecosystem exchange in three forest biomes. Global Change Biology 13, 776–787.

Alton, P., Ellis, R., Los, S., North, P., 2007b. Improved global simulations of Gross Primary Product based on a separate and explicit treatment of diffuse and direct sunlight. JGR 112, 07203.

Alton, P., 2008. Reduced carbon sequestration in terrestrial ecosystems under overcast skies compared to clear skies. Forest and Agricultural Meteorology 148, 1641–1653.

Alton, P., Fisher, R., Los, S., Williams, M., in press. Simulations of global evapotranspiration using semi-empirical and mechanistic schemes of plant hydrology, Global Biogeochemical Cycles.

Anderson, M., Norman, J., Meyers, T., Diak, G., 2000. An analytical model for estimating canopy transpiration and carbon assimilation fluxes based on canopy light use efficiency. Agricultural and Forest Meteorology 101, 265–289.

Asner, G., Scurlock, J., Hicke, J., 2003. Global synthesis of leaf area index observations: implications for ecological and remote sensing studies. Global Ecology & Biogeography 12, 191–205.

Baldocchi, D., Harley, P., 1995. Scaling carbon dioxide and water vapour exchange from leaf to canopy in deciduous forest. II. Model testing and application Plant. Cell and Environment 18, 1157–1173.

Baldocchi, D., Falge, E., Gu, L., 2001. FLUXNET: a new tool to study the temporatl and spatial variability of ecosystem-scale carbon dioxide, water vapour and energy flux densities. Bulletin of the American Meteorological Society 82, 2415–2434.

Ball, J., Woodrow, E., Berry, J., 1987. A model predicting stomatal conductance and its contribution to the control of photosynthesis under different environmental conditions, in: Biggins, J., Nijhoff, M. (Eds.), Progress in Photosynthesis Research. Dordrecht, Netherlands, pp. 221–224.

Barnsley, M., 2007. Environmental Modelling: A Practical Introduction. CRC Press, New York.

Barrett, D., 2002. Steady state turnover of carbon in the Australian terrestrial biosphere. Global Biogeochemical Cycles 16, 1108.

Bolstad, P., Davis, K., Martin, J., Cook, B., Wang, W., 2004. Component and whole-system respiration fluxes in northern deciduous forests. Tree Physiology 24, 493–504.

Campbell, B., Norman, J., 1998. Environmental Biophysics. Springer-Verlag, New York.

Carswell, F., Meir, P., Wandelli, E., 2000. Photosynthetic capacity in a central. Amazonian Rain Forest Tree Physiology 20, 179–186.

Choudhury, B., 2001. Estimating gross photosynthesis using satellite and ancillary data: approach and preliminary results. Remote Sensing of Environment 75, 1–21.

Collatz, G., Ball, J., Grivet, C., Berry, J., 1991. Physiological and environmental regulation of stomatal conductance, photosynthesis and transpiration: a model that includes laminar boundary layer. Agricultural and Forest Meteorology 54, 107–136.

Collatz, G., Ribas-Carbo, J., Berry, J., 1992. Coupled photosynthesis-stomatal conductance model for leaves of C4 plants. Australian Journal of Plant Physiology 19, 519–538.

Cosby, B.J., Hornberger, G.M., Clapp, R.B., Ginn, T.R., 1984. A statistical exploration of the relationship of moisture characteristics to the physical properties of soils. Water Resource Research 20, 682–690.

Cox, P., Huntingford, C., Harding, R., 1998. A canopy conductance and photosynthesis model for use in a GCM land surface scheme. Journal of Hydrology 212–213, 79–94.

Cox, P., Betts, R., Bunton, C., Essery, R., Rowntree, P., Smith, J., 1999. The impact of new land surface physics on the GCM simulation of climate and climate sensitivity. Journal of Climate Dynamics 15, 183–203.

Cox, P., 2001. Description of the TRIFFID dynamic global vegetation model Hadley Centre Technical Note 24, (Ed. Met. Office, Bracknell, UK) available on-line http://www.metoffice.gov.uk/research/hadleycentre/pubs/HCTN/HCTN_24.pdf.

Cramer, W., Bondeau, A., Woodward, F., 2001. Global response of terrestrial ecosystem structure and function to CO_2 and climate change: results from six dynamic global vegetation models. Global Change Biology 7, 357–373.

Dai, Y., Dickinson, R., Wang, Y., 2004. A two-big-leaf model for canopy temperature, photosynthesis, and stomatal conductance. Journal of Climate 17, 2281–2299.

Dang, Q., Margolis, H., Collatz, G., 1998. Parameterization and testing of a coupled photosynthesis-stomatal conductance model for boreal trees. Tree Physiology 18, 141–153.

Dirmeyer, P., Dolman, A., Sato, N., 1999. The global soil wetness project; a pilot project for global land surface modelling and validation. Bulletin of American Meteorological Society 80, 851–878. http://www.iges.org/gswp/.

Draper, N., Smith, H., 1981. Applied Regression Analysis. John Wiley and Sons, New York.

Falge, E., Tenhunen, J., Baldocchi, D., 2002. Phase and amplitude of ecosystem carbon release and uptake potential as derived from FLUXNET measurements. Agricultural and Forest Meteorology 113, 75–95.

Farquhar, G., von Caemmerer, S., Berry, J., 1980. A biochemical model of photosynthetic CO_2 assimilation in leaves of C_3 species. Planta 149, 78–90.

Field, C., Mooney, H., 1986. The photosynthesis-nitrogen relationship in wild plants. In: Givnish, T. (Ed.), On the economy of plant form and function. Cambridge University Press, Cambridge, pp. 25–55.

Fisher, J., Tu, K., Baldocchi, D., 2008. Global estimates of the land-atmosphere water flux based on monthly AVHRR and ISLSCP-II data, validated at 16 FLUXNET sites. Remote Sensing of Environment 112, 901–919.

Friend, A., Stevens, A., Knox, R., Cannell, M., 1997. A process-based, terrestrial biosphere model of ecosystem dynamics (Hybrid v3.0). Ecological Modelling 95, 249–287.

Friend, A., Arneth, A., Kiang, N., 2007. FLUXNET and modelling the global carbon cycle. Global Change Biology 13, 610–633.

Goetz, S., Prince, S., 1996. Remote sensing of net primary production in boreal forest stands. Agricultural and Forest Meteorology 78, 149–179.

Goulden, M., Munger, J., Fan, S., Daube, B., Wofsy, S., 1996. Measurements of carbon sequestration by long-term eddy covariance: methods and a critical evaluation of accuracy. Global Change Biology 2, 169–182.

Gower, S., Kucharik, C., Norman, J., 1999. Direct and indirect estimation of leaf area index, f_{APAR} and net primary production of terrestrial ecosystems. Remote Sensing of Environment 70, 29–51.

Gu, L., Fuentes, J.D., Shugart, H.H., Staebler, R.M., Black, T.A.T.A., 1999. Responses of net ecosystem exchanges of carbon dioxide to changes in cloudiness: results from two North American deciduous forests. Journal of Geophysical Research 104, 31421–31434.

Gu, L., Baldocchi, D., Verma, S., 2002. Advantages of diffuse radiation for terrestrial ecosystem productivity. Journal of Geophysical Research 107, 101029.

Heinsch, F., Zhao, M., Running, S., 1908–1925. Evaluation of remote sensing based terrestrial productivity from MODIS using regional tower eddy flux network observations. IEEE Transactions on Geoscience and Remote Sensing 44 .

Hendrickson, L., Ball, M., Wood, J., Chow, W., Furbank, R., 2004. Low temperature effects on photosynthesis and growth of grapevine. Plant Cell and Environment 27, 795–809.

Hirose, T., Werger, M., 1987. Maximising daily canopy photosynthesis with respect to leaf N allocation pattern in the canopy. Oecologia 72, 520–526.

Hollinger, D., Kelliher, F., Byers, J., Hunt, J., McSeveny, T., Wier, P., 1994. Carbon dioxide exchange between an undisturbed old-growth temperate forest and the atmosphere. Ecology 75, 134–150.

Hollinger, D., Richardson, A., 2005. Uncertainty in eddy covariance measurements and its application to physiological models. Tree Physiology 25, 873–885.

Houborg, R., Anderson, M., Norman, J., Wilson, T., Meyers, T., in press. Intercomparison of a bottom-up and top-down modeling paradigm for estimating carbon and energy fluxes over a variety of vegetative regimes across the U.S. Agricultural and Forest Meteorology. doi:10.1016/j.agrformet.2009.06.014.

Jackson, R., Canadell, J., Ehleringer, J., Mooney, H., Sala, O., Schulze, E., 1996. A global analysis of root distributions for terrestrial biomes. Oecologia 108, 389–411.

Janssen, P., Heuberger, P., 1995. Calibration of process oriented models. Ecololgical Modelling 83, 55–66.

Jones, H., 1992. Plant and Microclimate. Cambridge University Press, Cambridge.

Knohl, A., Baldocchi, D., 2008. Effects of diffuse radiation on canopy gas exchange processes in a forest ecosystem. Journal of Geophysical Research 113, 02023.

Knorr, W., Heimann, M., 2001. Uncertainties in global terrestrial biosphere modeling. Part I. A comprehensive sensitivity analysis with a new photosynthesis and energy balance scheme. Global Biogeochemical Cycles 15, 207–225.

Knorr, W., Kattge, J., 2005. Inversion of terrestrial ecosystem model parameter values against eddy covariance measurements by Monte Carlo sampling. Global Change Biology 11, 1333–1351.

Law, B., Ryan, M., Anthoni, P., 1999. Seasonal and annual respiration of a ponderosa pine ecosystem. Global Change Biology 5, 169–182.

Law, B., Falge, E., Gu, L., Baldocchi, D., Bakwin, P., Berbigier, P., Davis, K., Dolman, A., Falk, M., Fuentes, J., Goldstein, A., Granier, A., Grelle, A., Hollinger, D., Janssens, I., Jarvis, P., Jensen, N., Katul, G., Mahli, Y., Matteuccir, G., Meyers, T., Monson, R., Munger, W., Oechel, W., Olson, R., Pilegaard, K., Paw, K., Thorgeirsson, H., Valentini, R., Verma, S., Vesala, T., Wilson, K., Wofsy, S., 2002. Environmental controls over carbon dioxide and water vapour exchange of terrestrial vegetation. Agricultural and Forest Meteorology 113, 97–120.

Lewis, J., McKane, R., Tingey, D., Beedlow, P., 2000. Vertical gradients in photosynthetic light response within an old-growth douglas-fir and western hemlock canopy. Tree Physiology 20, 447.

Lloyd, J., Shibistova, O., Zolotoukhine, D., 2002. Seasonal and annual variations in the photosynthetic productivity and carbon balance of a central Siberian pine forest. Tellus 54B, 590–610.

Long, S., Hutchin, P., 1991. Primary productivity in grasslands and coniferous forests with climate change: an overview. Ecological Applications 12, 139–156.

Los, S., Pollack, N., Parris, M., 2000. A global 9-yr biophysical land surface dataset from NOAA AVHRR data. Journal of Hydrometeorology 1, 183–199.

de Lucia, E., Drake, J., Thomas, R., Gonzalez-Melers, M., 2007. Forest carbon use efficiency: is respiration a constant fraction of gross primary production? Global Change Biology 13, 1157–1167.

Lyons, T., 2002. Clouds prefer native vegetation. Meteorology Atmospheric Physics 80, 131–140.

Medlyn, B., Barrett, D., Landsberg, J., Sands, P., Clement, R., 2003. Conversion of canopy-intercepted radiation to photosynthate: review of modelling approaches for regional scales. Functional Plant Biology 30, 153–169.

Medlyn, B., Robinson, A., Clement, R., McMurtie, E., 2005. On the validation of models of forest CO_2 exchange using eddy covariance data: some perils and pitfalls. Tree Physiology 25, 839–857.

Meir, P., Kruijt, B., Broadmeadow, M., 2002. Acclimation of photosynthetic capacity to irradiance in tree canopies in relation to leaf N concentration and leaf mass per unit area. Plant Cell and Environment 25, 343–357.

Mercado, L., Huntingford, C., Gash, J., Cox, P., Jogireddy, V., 2007. Improving the representation of radiation interception and photosynthesis for climate model application. Tellus B 59, 553–569.

Mercado, L., Bellouin, N., Sitch, S., Boucher, O., Huntingford, C., Wild, M., Cox, P., 2009. Impact of changes in diffuse radiation of the global land carbon sink. Nature 458, 1014–1018.

Misson, L., Panek, J., Goldstein, A., 2004. A comparison of three approaches to modelling leaf gas exchange in annually drought-stressed ponderosa pine forests. Tree Physiology 24, 529–541.

Monteith, J.L., 1965. Evaporation and environment. Symposia of the Society for Experimental Biology 19, 205–234.

Monteith, J.L., 1977. Climate and the efficiency of crop production in Britain. Transactions of the Royal Society of London Series B 281, 277–294.

Newman, E., 1969. Resistance to water flow in soil and plant. I. Soil resistance in relation to amounts of root: theoretical estimates. Journal of Applied Ecology 6, 1–12.

Niyogi, D., 2004. Direct observations of the effects of aerosol loading on net ecosystem CO_2 exchanges over different landscapes Geophy. Research Letters 31, 3120506.

Norcliffe, G., 1977. Inferential Statistics for Geographers. Hutchinson and Co, London.

Norman, J., 1981. Interfacing Leaf and canopy light interception models, in: Hesketh, J., Jones, J. (Eds.). Predicting Photosynthesis for Ecosystem Models 49–67, CRC Press, Boca Raton, FL.

Potter, C., Randerson, J., Field, C., Matson, P., Vitousek, P., Mooney, H., Klooster, S., 1993. Terrestrial ecosystem production: a process model based on global satellite and surface data. Global Biogeochemical Cycles 7, 811–841.

Press, W., Teukolsky, S., Vetterling, W., Flannery, B., 1992. Numerical Recipes: The Art of Scientific Computing. Cambridge University Press, Cambridge.

Raich, P., 1992. The global carbon dioxide flux in soil respiration and its relationship to vegetation and climate. Tellus 44B, 81–99.

Ramirez, J., Senarath, S., 2000. A statistical-dynamical parameterization of canopy interception and land surface-atmosphere interactions. Journal of Climate 13, 4050–4063.

Raupach, M., Finnigan, J., 1988. Single layer models of evaporation from plant canopies are incorrect but useful, whereas multilayer models are correct but useless. Australian journal of plant physiology 15, 705–716.

Reichstein, M., Tenhunen, J., Roupsard, O., 2003. Inverse Modelling of seasonal drought effects on canopy CO_2/H_2O exchange in three Mediterranean ecosystems. JGR 108 (D23), 4726.

Roderick, M., Farquhar, G., Berry, S., Noble, I., 2001. On the direct effect of clouds and atmospheric particles on the productivity and structure of vegetation. Oecologia 129, 21–30.

Ruimy, A., Kergoat, L., Bondeau, A., 1999. Comparing global models of terrestrial net primary production (NPP): analysis of differences in light absorption and light-use efficiency. Global Change Biology 5, 56–64.

Running, S., Coughlan, J., 1988. A general-model of forest ecosystem processes for regional applications: 1. Hydrologic balance, canopy gas-exchange and primary production processes. Ecological Modelling 42, 125–154.

Running, S., Nemani, R., Heinsch, F., Zhao, M., Reeves, M., Hashimoto, H., 2004. A continuous satellite-derived measure of global terrestrial primary production. Bio Science 54, 547–560.

Ryan, M., 1991a. A simple method for estimating gross carbon budgets for vegetation in forest ecosystems. Tree Physiology 9, 255–266.

Ryan, M., 1991b. The effects of climate change on plant respiration. Ecological Applications 1, 157–167.

Schlesinger, W., 1997. Biogeochemistry: An Analysis of Global Change. Academic Press, San Diego.

Schrader, S.M., Wise, R.R., Wacholtz, W.F., Ort, D.R., Sharkey, T.D., 2004. Thylakoid membrane responses to moderately high leaf temperature in Pima cotton. Plant, Cell and Environment 27, 725–736.

Schulze, E-D., Kelliher, F., Korner, C., Lloyd, J., Leuning, R., 1994. Relationships amoung maximum stomatal conductance, ecosystem surface conductance, carbon assimilation rate and plant nitrogen nutrition: a global ecology scaling exercise. Annual Review of Ecology and Systematics 25, 629–660.

Sellers, P., Meeson, B., Hall, F., 1995. Remote sensing of the land surface for studies of global change: model-algorithms-experiments. Remote Sensing of Environment 51, 3–26.

Sellers, P., Randall, D., Collatz, G., 1996a. A revised land surface parameterization (SiB2) for atmospheric GCMs. Part I. Model formulation. Journal of Climate 9, 676–705.

Sellers, P., Los, S., Tucker, C., Justice, C., Dazlich, D., Collatz, G., Randall, D., 1996b. A revised land surface parameterization (SiB2) for atmospheric GCMs. Part II. The generation of global fields of terrestrial biophysical parameters from satellite data. Journal of Climate 9, 706–737.

Sellers, P., Dickinson, R., Randall, D., 1997. Modeling the exchanges of energy, water and carbon between continents and the atmosphere. Science 275, 502–509.

Sheffield, J., Goteti, G., Wood, E., 2006. Development of a 50-year high-resolution global dataset of meteorological forcings for land surface modelling. Journal of Climate 19, 3088–3111.

Sims, D., Rahman, A., Cordova, V., Baldocchi, D., Flanagan, L., Goldstein, A., Hollinger, D., Misson, L., Monson, R., Schmid, H., Wofsy, S., Xu, L., 2005. Midday values of gross CO_2 flux and light-use efficiency during satellite overpasses can be used to directly estimate eight-day mean flux. Agricultural and Forest Meteorology 131, 1–12.

Singsaas, E., Ort, D., DeLucia, E., 2001. Variation in measured values of photosynthetic quantum yield in ecophysiological studies. Oecologia 128, 15–23.

Tjoelker, M.G., Oleksyn, J., Lee, T.D., Reich, P.B., 2001. Direct inhibition of leaf dark respiration by elevated CO_2 is minor in 12 grassland species. New Phytology 150, 419–424.

Udo, S., Aro, T., 1999. Global PAR related to global solar radiation for central Nigeria. Agricultural and Forest Meteorology 97, 21–31.

Wang, Y., Leuning, R., Cleugh, H., Coppin, P., 2001. Parameter estimation in surface exchange models using nonlinear inversion; how many parameters can we estimate and which measurements are most useful? Global Change Biology 7, 495–510.

Waring, R.H., Landseberg, J.J., Williams, M., 1998. Net primary production of forests: a constant fraction of gross primary production? Tree Physiology 18, 129–134.

Williams, D., 1991. A comparison of spectral reflectance properties at the needle, branch and canopy level for selected conifer species Remote Sens. Environ. 35, 79–93.

Wong, S., Cowan, I., Farquhar, G., 1979. Stomatal conductance correlates with photosynthetic capacity. Nature 282, 424–426.

Yuan, W., Liu, S., Zhou, G., 2007. Deriving a light-use efficiency model from eddy covariance flux data for predicting daily gross primary production across biomes. Agricultural and Forest Meteorology 143, 189–207.

Zaehle, S., Sitch, S., Smith, B., Hatterman, F., 2005. Effects of parameter uncertainties on the modeling of terrestrial biosphere dynamics. Global Biogeochemical Cycles 19, G3020.

Zhao, M., Heinscha, F., Ramakrishna, R., Nemani, B., Running, S., 2005. Improvements of the MODIS terrestrial gross and net primary production global data set. Remote Sensing of Environment 95, 164–176.